Rapid microwave synthesis of tetrahedral pyrazole/Co(II) complex: [N—H···Cl] synthon, XRD/HSA-interactions, DFT/TD-DFT, physiochemical, antifungal, antibacterial, and POM bio-calculations

Abderrahim Titi [a], Ismail Badran [b], Mohammed Dahmani [c], Mouslim Messali [d], Rachid Touzani [a], Abdelkader Zarrouk [e], Yann Garcia [f], Mousa Al-Noaimi [g], Mohammed Suleiman [b], Ismail Warad [b,*]

[a] *Laboratory of Applied and Environmental Chemistry (LCAE), Mohammed first University, Oujda, Morocco*
[b] *Department of Chemistry, An-Najah National University, P.O. Box 7, Nablus, Palestine*
[c] *Laboratory of Applied Chemistry and Environment–ECOMP, Faculty of Sciences, Mohammed First University Bd Mohamed VI, BP: 717, Oujda 60000, Morocco*
[d] *Department of Chemistry, College of Science, Imam Mohammad Ibn Saud Islamic University, P.O. Box 90950, Riyadh 11623, Saudi Arabia*
[e] *Laboratory of Materials, Nanotechnology, and Environment, Faculty of Sciences, Mohammed V University in Rabat, P.O. Box. 1014 Agdal-Rabat, Morocco*
[f] *Institute of Condensed Matter and Nanosciences, Molecular Chemistry, Materials and Catalysis (IMCN/MOST), Université catholique de Louvain, Place L. Pasteur 1, 1348 Louvain-la-Neuve, Belgium*
[g] *Chemistry Department, Faculty of Science, Kuwait University, P.O. Box 5969, Safat 13060, Kuwait*

ARTICLE INFO

Keywords:
Pyrazole
Co(ii) complex, xrd, dft, biological, pom theory

ABSTRACT

A new coordination complex, $CoCl_2(NNH)_2$, was synthesized by complexation of the pyrazole (NNH) ligand with $CoCl_2$ in less than 5 min with a high yield (>85%). The synthesis was done using microwave radiation in water solvent where no side products were detected. The complexation was confirmed using UV–visible, CHN-analysis, and FT-IR analysis and compared to theoretical IR, DFT and TD-DFT calculations. $CoCl_2(NNH)_2$ crystallizes in a C2/c space group with distorted tetrahedral center as shown by single-crystal X-ray diffraction, two types of heteromeric [N—H···Cl] synthons have been recorded, such interactions type and ratios were confirmed also via Hirsfield surface analysis (HSA). The desired complex was evaluated for its antibacterial activity against four classes of *gram-positive* and *gram-negative bacteria*, and its antifungal activity against four types of *fungi*. The complex's physio-chemical properties, toxicity risk, lipophilicity, and pharmacophore sites were studied using the POM (Petra-Osiris-Molinspiration) bio-computational theory.

1. Introduction

Pyrazole and its derivatives molecules are considered to be one of the most important types of *O,N*-heterocyclic molecules. They are widely used in the synthesis of many organic compounds and hybrid materials [1–6]. Because of their diverse biological activities, they are considered promising therapeutic agents in anticancer, antibacterial, antifungal, antimalarial, medicine, agriculture, polymer industries, and bio-inorganic chemistry [7–10]. For example, the pyrazole ring is an essential part of several accessible pharmaceutical drugs such as Celecobix, Doramapimod, and 32,945-PNU [11,12]. The pyrazole derivatives have an excellent capacity to coordinate with transition metals that can be used for the fabrication of materials with specific properties, especially in the capture and conversion of CO_2, energy-storage, and in selective catalysis [13,14]. Some of the pyrazole ligands are featured by specific sites that gives them the capabilities to coordinate strongly with heavy metals. The design and synthesis of these compounds, with such properties, will be critical in solving many problems, particularly in water cleaning as metal ions extractors [15–18].

The addition of various organic substituents to the pyrazole ring has the potential to improve important properties such as chelation, stability, water solubility, and biological activities, so there is a growing interest in pyrazole chelating molecules decorated with N, O, and P heteroatom donors [39–40]. The ability to modify the pyrazole ring in this way has increased research in this area and holds promise for improved materials with a variety of potential applications [3–8].

* Corresponding author.
E-mail address: warad@najah.edu (I. Warad).

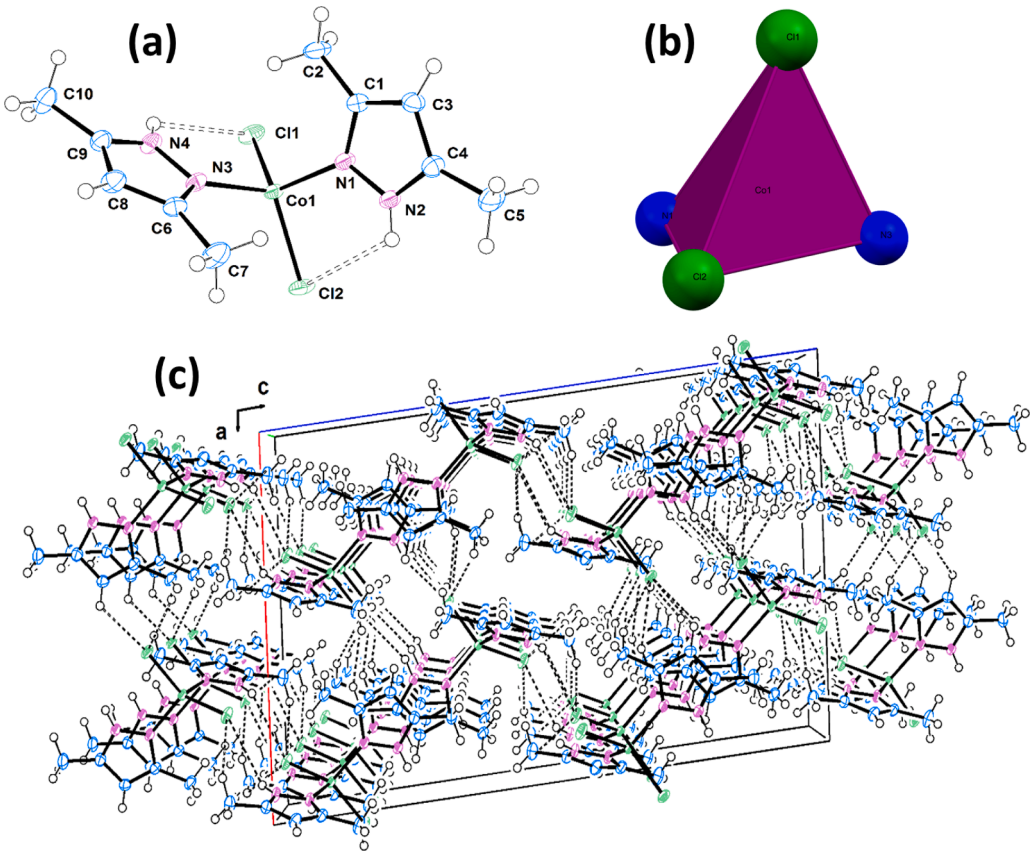

Fig. 1. (a) ORTEP diagram, (b) *Td* coordination environment, and (c) Molecular packing and hydrogen bonding interactions in desired complex.

The synthesis of pyrazole derivatives and their coordination with transition metals has been widely studied, leading to the characterization of their structures, physical and chemical properties, spectra, thermal behavior, catalytic activities, and biological activities [1–6]. The complexation structures and the location of active sites in hybrid materials can be affected by the three-dimensional structure of the materials, leading to a diverse range of properties [2–6].

In this work, neutral Co(II) complexes coordinated to two pyrazole ligands were synthesized, the 3D-structure, spectroscopic, thermal, and biological activity were investigated. Here, we use the sustainable and eco-friendly green microwave approach to create and thoroughly describe a novel Tetrahedral $CoCl_2(NNH)_2$ complex. The physicochemical experimental analyzes of the title complex were accompanied by the DFT calculations in order to prove the molecular structure and verify the degree of convergence between experimental measurements and theoretical calculations. Additionally, the intended complex's biological characteristics and POM bio-computation have been assessed.

2. Experimental

2.1. Materials and physical measurement

The $CoCl_2(NNH)_2$ complex was prepared by reacting (NNH) 3,5-methyl-1H-pyrazole and Co(II) chloride in water under microwave irradiation using a CEM discovery controllable single-mode microwave reactor under a pressure of 2×10^6 Pa and power of 300 W. The complexation was followed by IR spectroscopy at room temperature with a Perkin Elmer FT-IR spectrometer in the range of 4000–400 cm^{-1}. The UV-visible measurements were carried out on TU-1901 double-beam UV–Vis. spectrophotometer. Bio-calculations were performed by using POM Platform [7,8,19,20].

2.2. Synthesis of $CoCl_2(NNH)_2$ complex

An aqueous NNH ligand solution (1 mmol in 10 mL) was mixed into an aqueous $CoCl_2{\cdot}6H_2O$ solution (0.5 mmol in 10 mL). The reaction mixture was directly moved to a closed vessel and placed in a microwave for a period of 5 min. The resulting red solution was filtered to eliminate undesired solid impurities and left for evaporation under ambient conditions. After two days, red plates of $CoCl_2(NNH)_2$ were formed (yield $\geq$85%). Selected IR band: ν = 3358 (N—H), 3058 (C_{Pyr}-H), 2947 (C_{Me}-H), 1678 (C = N), 1484 (C = C), 1373 (N—N), 450 (Co-N) cm^{-1}.

2.3. Antibacterial and antifungal studies

Antibacterial studies of the $CoCl_2(NNH)_2$ complex were evaluated against four famous Gram-positive bacteria (*Aspergillus flavus, Penicillium Marneffeii, Candida albicans Cryptococcus neoformans*, and two class of Gram-negative bacteria (*Escherichia coli* and *Proteus vulgaris*. The agar-well diffusion approach was used, with gentamycin as a reference, as reported in our previous published works [7,20]. The wells (6 mm in diameter) were drug in the media with the help of a sterile metallic borer. Bacterial inocula (2–8 h old) containing approximately 102–104 colony-forming units (CFU/mL) were spread on the surface of the nutrient agar with the help of a sterile cotton swab. The recommended concentration of the test sample (1 mg/mL in DMSO) was introduced in the respective wells. Other wells supplemented with DMSO and reference antibacterial drug, *Gentamycin* served as negative and positive controls, respectively. The plates were incubated at 37 °C for 24 h. The activity was determined by measuring the diameter of zones showing complete inhibition (mm).

In order to evaluate the interfering effect of DMSO on the biological screening, alternative studies on DMSO solution showed no activity against any bacterial strains. In addition, antifungal activities of the

Table 1
Selected angles [°] and bond lengths [Å] for $CoCl_2(NNH)_2$.

No.	Angles	[°]	No.	Bonds	Å
1	N(3)-Co(1)-N(1)	106.66(7)	1	Co(1)-N(1)	2.0040(16)
2	N(3)-Co(1)-Cl(1)	100.34(4)	2	Co(1)-N(3)	2.0030(16)
3	N(1)-Co(1)-Cl(1)	114.58(5)	3	Co(1)-Cl(1)	2.2457(5)
7	C(1)-N(1)-N(2)	105.60(15)	7	N(2)-C(4)	1.342(2)
8	C(1)-N(1)-Co(1)	129.88(12)	8	N(3)-C(6)	1.339(2)
9	N(2)-N(1)-Co(1)	124.16(11)	9	N(3)-N(4)	1.3624(19)
10	C(4)-N(2)-N(1)	111.68(14)	10	N(4)-C(9)	1.338(3)
11	C(6)-N(3)-N(4)	105.35(15)	11	C(1)-C(3)	1.395(3)
12	C(6)-N(3)-Co(1)	133.19(12)	12	C(3)-C(4)	1.380(2)
13	N(4)-N(3)-Co(1)	121.39(12)	13	C(6)-C(8)	1.393(3)
14	C(9)-N(4)-N(3)	111.88(15)	14	C(8)-C(9)	1.375(3)

Symmetry code: #1 = -x + 1,-y + 1,-z + 1.

prepared complex were tested, against four types of fungi [*Aspergillus flavus, Penicillium Marneffeii, Candida albicans* and *Cryptococcus neoformans]* following the same protocol descripted in the literature [20].

Sabouraud dextrose agar (Oxoid, Hampshire, England) was seeded with 105 (cfu) mL^{-1} fungal spore suspensions and transferred to petri plates. Discs soaked in 20 mL (200 μg /mL in DMSO) of the compounds were placed at different positions on the agar surface. The plates were incubated at 32 °C for 7 days. The results were recorded as percent of inhibition and compared with the standard drug *Ketoconazole*.

2.4. X-ray structure determination

Single-crystal X-ray data for the prepared complex was collected on a Bruker D8 Quest diffractometer (Mo Kα radiation λ = 0.71073 Å). The data were collected and integrated using the Bruker APEX3 software package [21]. Multi-scan absorption correction was performed using SADABS [22]. The structure was solved by direct methods refined using full-matrix least squares procedures on F^2 via the program SHELXL-2014 [23]. The data was using ORTEP3 [24]. The isotropic displacement parameters were $U_{iso}(H) = 1.2U_{eq}(C)$ for methylene groups and sp^2 carbons and $U_{iso}(H) = 1.5U_{eq}(C)$ for methyl groups. For the pyrazole N—H bond in (**2**), $U_{iso}(H) = 1.2U_{eq}(N)$. The crystal data and refinement details for desired complex are given in **Table S1**.

2.5. Theoretical calculations

The MN15L Minnesota functional [25], and the 6–31+*G*(d,p) basis set were used to optimize the $CoCl_2(NNH_2)_2$ complex. The MN15L functional demonstrated excellent performance in describing similar systems [26–29]. Following each optimization, frequency calculations were performed to ensure that no imaginary frequencies were present. The Co(II) configuration was found to have a Td-structure with a spin multiplicity of doublet. As a result, unrestricted SCF was used by adding the prefix –u in the Gaussian input [26,30,31]. The excited states were probed by TD-DFT at the same level of calculation. More details on the theoretical calculations in this work can be found elsewhere [32–38]. All calculations were performed with Gaussian 16 Rev C.01 [33], and viewed with Gaussview [34].

3. Result and discussion

3.1. Synthesis of $CoCl_2(NNH)_2$ complex

The synthesis of $CoCl_2(NNH_2)_2$ complex has been achieved through microwave irradiation, which is recognized as an environmentally friendly process. The one-pot R.T. aqua-complexation method made the synthesis of the complex efficient, sustainable and environmentally-friendly. The reaction was done by mixing two equivalents of NNH ligand with one equivalent of $CoCl_2{\cdot}6H_2O$ in water under microwave irradiation at ambient conditions. This procedure allowed the formation of the desired complex in less than 5 min, as opposed to the long 24 h reported method, which required refluxing for more than 6 h [1].

Table 2
Hydrogen bonding geometry of $CoCl_2(NNH)_2$ [Å and °].

D-H…A	d(D-H)	d(H···A)	d(D···A)	<(DHA)
N(2)-H(2)…Cl(2)	0.860	2.914	3.386(2)	116.48
N(2)-H(2)…Cl(2)#4	0.860	2.602	3.422(2)	159.56
N(4)-H(4)…Cl(1)	0.860	2.773	3.288(2)	119.95
N(4)-H(4)… Cl(1)#5	0.860	2.876	3.459(2)	126.70
C(2)-H(2B)…Cl(2)#6	0.960	2.730	3.635(2)	157.25
C(5)-H(5A)…Cl(2)#4	0.960	2.980	3.817(2)	146.44

Symmetry codes: #1= -x + 1,-y + 1,-z + 1; #2 = x + 1, y, z; #3= -x + 1, y + 1/2,-z + 1/2.
#4 = -x + 1, y, -z + 1/2; #5 = -x + 3/2, -y + 3/2, -z + 1 ; #6 = x + 1/2, y-1/2, z.

3.2. Molecular structure

The ORTEP structure of complex is given in Fig. 1 together with selected geometrical parameters (Table 1) and H-bonds interactions (Table 2). The $CoCl_2(NNH)_2$ complex crystallizes in the C2/c space group. The cobalt(II) ion is bound to two nitrogen atoms, each belonging to a pyrazole ligand, in addition to two chloride anions (Fig. 1a), in a slightly distorted tetrahedral geometry with τ = 0.96 (Fig. 1b). The methyl groups found to be in the same plane of five-membered ring of the pyrazole ligand as seen in Fig. 1a. The average Co-N and Co-Cl bond lengths are 2.004(2) Å and 2.2469(5) Å, respectively. Moreover, the bond angles around the metal ion are in the range of 100.34(4)°-119.77 (2)°, consisting with similar reported complexes [25,26]. Intramolecular H-bonds interactions (N—H···Cl) take place, inducing relatively low torsion angles Cl1-Co1-N3-N4 (−3.4 (1)°) and Cl2-Co1-N1-N2 (−12.9 (1)°). These interactions are likely to decrease the bond angles N3-Co1-Cl1 and N1-Co1-Cl2 to 100.34(4)° and 100.78(4)°, respectively. The molecules of the complex are packed to form columns along the *b*-axis and are involved in a 3D intermolecular hydrogen bonding (N—H···Cl) interaction scheme (Fig. 1c).

3.3. Heteromeric R_2^2 (10) [N—H···Cl] synthon

A synthon was observed in the complex's lattice, and refers to the non-coordinated payroll N—H and Cl atoms of a nearby complex involving complementary N—H···Cl 2D hydrogen bonded network. This results in the formation of two dimer complexes per each molecule (Fig. 2a), via two heteromeric R_2^2 (10) with bond distance = 2.676 Å (Fig. 2b). Such type of synthon plays a significant role in the thermal stabilization of the crystal lattice orientation that contributes to the overall stability and symmetry of the lattice. Moreover, such synthon controls the physical and chemical properties of the crystal. One other hand, two one-dimensional hydrogen bonded network per each molecule are formed via non-classical C_{Me}-H···Cl bonds, with distance = 2.730 Å, as illustrated Fig. 2c.

3.4. Hirshfeld surface analysis (HSA)

The intermolecular interactions in the crystal lattice of $CoCl_2(NNH)_2$ can be studied quantitatively using HSA. The Crystal Explorer 3.1 software was used to plot the fingerprint plots of the Hirshfeld surfaces [1–5]. The d_{norm}, which was calculated using a static color scale of −0.28 (red) to 1.28 (blue) with high surface resolution was used to display the maps. Three red peaks can be seen in the d_{norm} surface (Fig. 3a). This represents the hydrogen bonding connections in the complex's lattice. The chlorine atoms form the first classical hydrogen bonds with the nearby H—N, and non-classical hydrogen bond H—C_{Me} with distances of 2.61 and 2.74 Å, respectively. Two types of hydrogen bonds interaction have been confirmed by HSA analysis which is consistent with the XRD result. Additionally, it is possible to determine

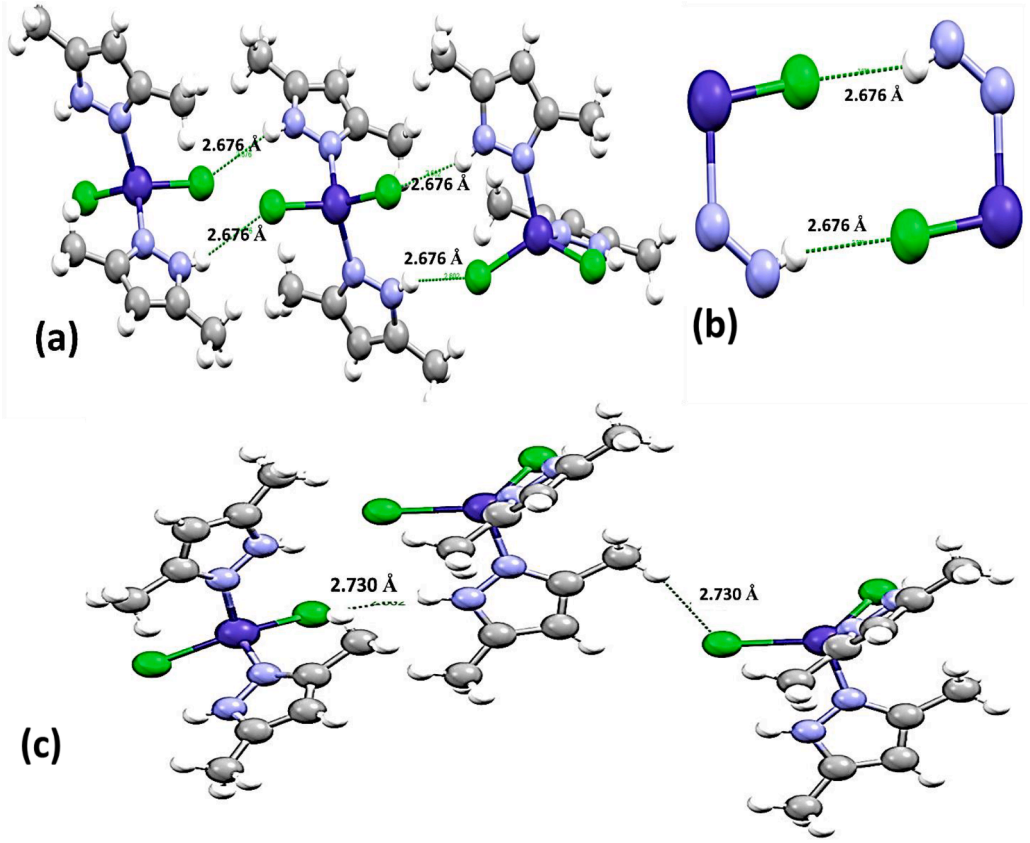

Fig. 2. (a) 2D N—H···Cl H-bonded network, (b) R_2^2 (10) synthons, and (c) 1D network 1D C_{Me}-H···Cl interactions.

the electronic density of the complex's constituent atoms using the shape index (Fig. 2b). This neutralizes the electronic map of the compound's surface which showed that the chlorine atoms have electronic rich centers (red), whereas the hydrogen atoms have electronic poor centers (blue). Moreover, the 2D-FP/HSA interaction ratios plots, the major contribution has been cited to H···H interaction with 52.6%. A significant contribution from Cl···H contacts is represented by 11.2%, whereas the other fingerprint plots are given in Fig. 2c.

3.5. FT-IR analysis

The IR spectra of NNH free ligand and its $CoCl_2(NNH)_2$ complex display the most important functional groups such as N—N, N=C, C=C aromatic, N—H, C—C, C—H aliphatic, as well as Co-N (Fig. 1S).

A significant change in the amine N—H group stretching vibration served as evidence that the coordination reaction of Co(II) with the N of sp2-hybridization and not its neighbor NH of sp3-hybridization atom was successful, from 3142 cm^{-1} (Fig. 1Sa) to higher wavenumber ~ 3309 cm^{-1} (Fig. 1Sb), and 1573 (Fig. 1Sa) to 1556 cm^{-1} (Fig. 1Sb) of C=N group, and appearance of novel signal of Co-N at 427 cm^{-1}. These findings were consistent with the XRD result and confirmed by DFT calculations (Fig. 1Sc). The figure shows the theoretical IR spectrum of the $CoCl_2(NNH)_2$ complex as obtained at uMN15L/6–31+g(d,p) level of theory. In fact, the strong band at ~ 3400 cm^{-1} is made up of two adjacent peaks corresponding to symmetric and asymmetric N—H bond stretching, shown at 3586 and 3595 cm^{-1} in the theoretical IR spectrum. The free ligand and its complex are essentially solid in their natural form, although theoretical DFT often compute in the gaseous state, which may account for the minor change in the theoretical and experimental IR spectra [26–29]. The experimental peak at ca.1550 was assigned to the C = N bond stretching, as confirmed by theoretical calculations. The peak at ca. 3000 cm^{-1}, on the other hand, is due to C—H vibrational in the terminal methyl groups.

3.6. UV–Visible and td-dft

The spectrum of the NNH ligand displays a significant band at λ_{max} = 342 nm, which is attributed to the free π-π* electronic transition (**Fig. 2Sa**). Upon mixing of the NNH ligand with Co(II) in EtOH, under MW irradiation, the color turned blue as expected from the complexation reaction. The spectrum of the prepared complex displays two broad bands (**Fig. 2Sb**). The most prominent one located at λ_{max}= 645 nm, is related to the D-d electronic transition of the tetrahedral Co(II) center. The second band at λ_{max}= 348 nm corresponds to the ligand π-π* transition. To better understand the electronic transitions within our complex, TD-DFT calculations were performed (Fig. 2Sd). The theoretical spectrum agrees very well with the experimental one, which reflects the good performance of the MN15L functional [26-29,35]. The peak at λ_{max}= 350 nm is the result of electronic excitations within the ligand molecule structure. According to our TDDFT calculations, the most intense electronic transitions are listed in Table 3. Clearly, the strongest transition is originating from the 19th excited state with an oscillator strength (f) of 0.493, at a wavelength of 329.7 nm, with an excellent agreement with the λ_{max} = 348 nm of the experimental spectrum. The first electronic transition also has an S^2 value of 2, indicating a pure *doublet* multiplicity. Other transitions in the range of 320–400 nm also contribute to the observed spectrum (Table 3). The molecular orbital diagram of the complex is shown in Fig. 2Sd, with the HOMO and LUMO listed as number 82 and 83 orbital numbers, respectively. The HOMO and LUMO shapes are also shown in Fig. 2Sd. A deep look at excited transitions in Table 3 reveals that the most intense excited state, #19, is actually a result of an electronic transition from the HOMO-1→LUMO+2. Both molecular orbitals are illustrated in Fig. 2Sd. The electron density distribution in this transition clearly shows an electron

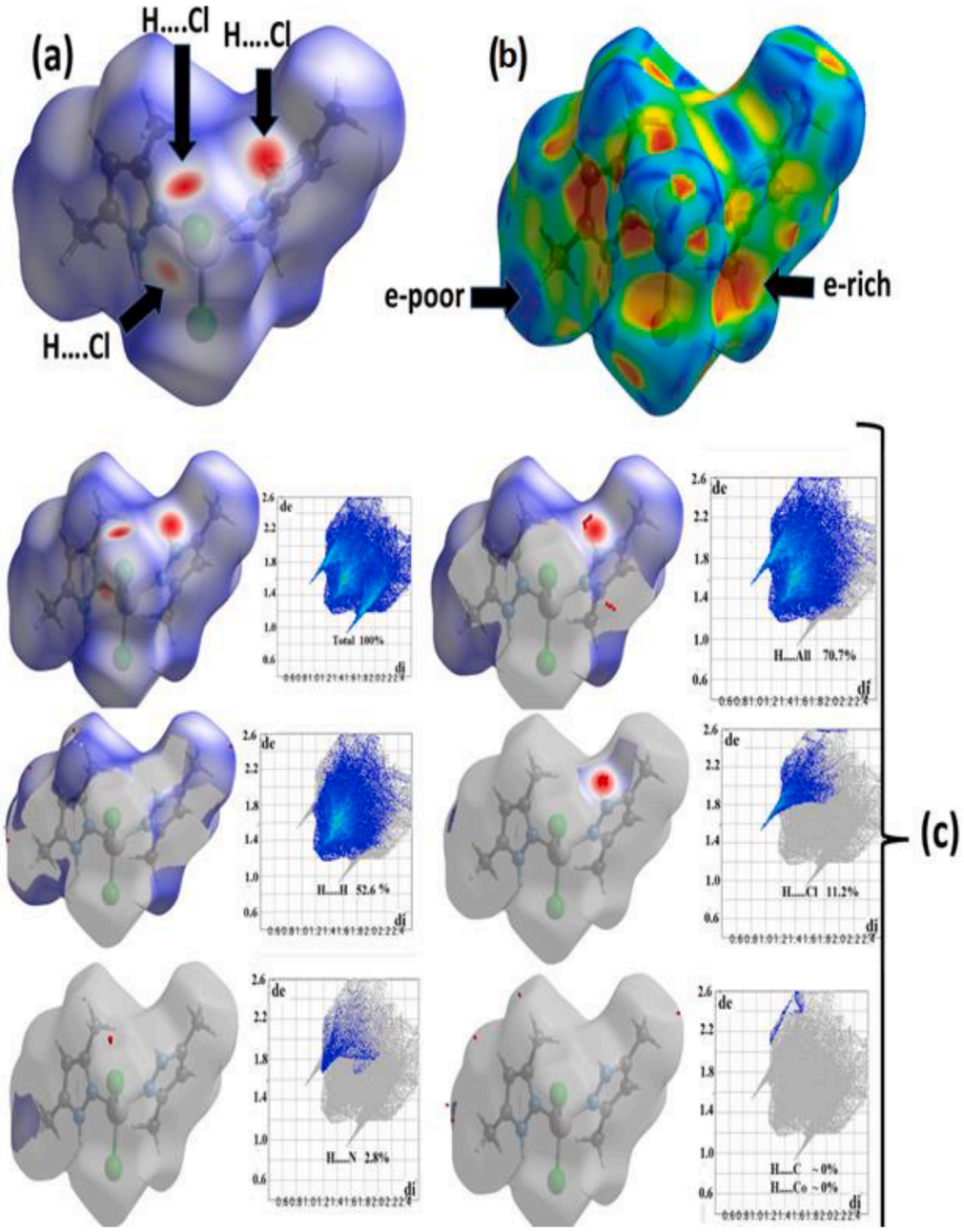

Fig. 3. (a) d_{norm}, (b) shape-index and (c) 2D-FP of $CoCl_2(NNH)_2$.

Table 3
Types and origins of electronic excitations performed at uMN15L/6–31+*G*(d) level of theory.

No.	Excitation band	λ (nm)	Energy gap (eV)	Oscillator Strength (f)	S^{2**}
19	HOMO-64	329.7	3.760	0.0493	1.99
10	HOMO-73	498.4	2.488	0.0197	1.81
17	HOMO-66	336.5	3.684	0.0161	1.96
21	HOMO-62	320.8	3.865	0.0096	1.84
20	HOMO-63	323.5	3.832	0.0095	1.78
18	HOMO-65	334.7	3.704	0.0079	2.10
12	HOMO-71	482.5	2.570	0.0066	1.62
8	HOMO-77	611.0	2.029	0.0053	0.92

** S^2 indicates spin multiplicity. Pure vales of 0.0. 0.75, or 2.00 refer to singlet, doublet, or triplet excited states, respectively. Deviation from pure values indicates spin contamination.

density redistribution from the cobalt center to the aromatic pyrazole rings.

3.7. Antibacterial and antifungal evaluations

The results of the study indicate that the $CoCl_2(NNH)_2$ complex has significant potential as an antimicrobial agent. The complex was tested against a variety of microorganisms, including fungi and bacteria, and showed promising actives against most of the microorganisms tested.

In terms of antibacterial activity, the complex demonstrated strong potential against the *Gram-positive bacterium Bacillus subtilis*, with the best inhibition value of **22∓0.67 mm**, which was with significant value compared to *gentamycin* as drug reference **25∓1.33 mm**, as seen in Fig. Fig. 3Sa, meanwhile only **14∓1.33 mm** compared to *gentamycin* **30∓1.00 mm** when *Gram-positive Staphylococcus aureus bacterium was* applied. However, the complex showed weaker activity against the *Gram-negative, bacterium* with an inhibition value of **13∓0.67 mm**,

Table 4
Mol-inspiration calculations of **$CoCl_2(NNH)_2$**.

Compd.	Calculation of Molecular Properties [a]				Calculation of Bioactivity Scores [b]					
	TPSA	NONH	NV	VOL	GPCRL	ICM	KI	NRL	PI	EI
$CoCl_2(NNH)_2$	35	2	0	250	−0.31	−0.11	−0.32	−0.53	−0.43	−0.18
SD[1]	69	0	1	452	0.26	−0.14	−0.17	−0.32	−0.21	0.15
SD[2]	199	11	2	450	0.34	0.19	0.18	−0.06	0.66	0.46

[a] TPSA: Total molecular polar surface area, NONH: number of OH—N or O–NH interaction, NV: number of violations of five Lipinsky rules VOL: volume.
[b] GPCRL: GPCR ligand; ICM: Ion channel modulates; KI: Kinase inhibitor; NRL: Nuclear receptor ligand; PI: Protease inhibiter, El: Enzyme inhibitor. SD[1]:Ketoconazole and SD[2]: Gentamycin.

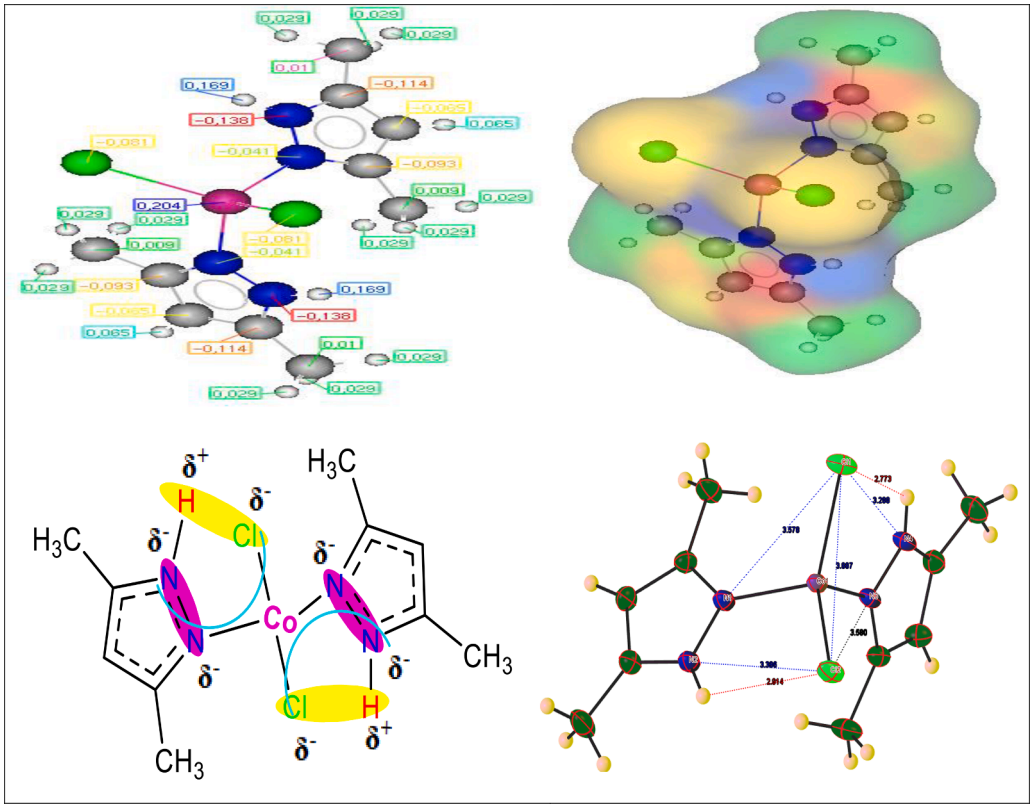

Fig. 4. Atomic charge and identification of pharmacophore sites of $CoCl_2(NNH)_2$.

compared to **30∓0.99 mm** and **20∓1.67 mm** compared to **25∓1.00 mm** inhibition using gentamycin as a reference for both *E. coli* and Proteus vulgaris strain respectively (Fig. 3Sa).

In general, the complex showed more activity against fungi than bacteria, as the inhibition values were usually close to the reference. the complex exhibited strong inhibitory effects against all four fungi species tested, with inhibition values ranging from (**12–25∓2.33 mm**). For example, *Cryptococcus neoformans* was found to be the most sensitive fungi, with an inhibition value of **25∓1.33 mm** comparable to **25∓1.67 mm** ketoconazole antifungal reference as can be seen in Fig. 3Sb

These results suggest that the $CoCl_2(NNH)_2$ complex has the potential to be developed into a new antimicrobial agent. The complex's ability to inhibit the growth of various microorganisms, including both *Gram-positive and Gram-negative* bacteria, as well as fungi, indicates a broad spectrum of activity. Furthermore, the complex showed similar or higher activity than the reference antibiotics tested, suggesting that it

Table 5
Osiris calculations of toxicity risks of **$CoCl_2(NNH)_2$**.

Compd.	MW	**Toxicity Risks** [a]				**Osiris calculations** [b]			
		MUT	TUM	IRRI	REP	cLogP	cLogS	DL	DS
$CoCl_2(NNH)_2$	322					0.9	−5.37	0.12	0.30
SD[1]	463					−4.55	−1.26	2.90	0.77
SD[2]	531					3.36	−2.99	8.14	0.60

Higly toxic ( ), Slightly toxic ( ), Not toxic ( ).
[a] **MW:** Molecular Weight, **MUT**: Mutagenic, **TUM**: Tumorigenic, **IRRIT**: Irritant, **RE**: Reproductive effective.
[b] **Sol**: Solubility, **DL**: Drug likeness, **DS**: Drug-Score, **ClogP**: Lipophilicity, **SD[1]**: Gentamycin, **SD[2]**: Ketoconaz.

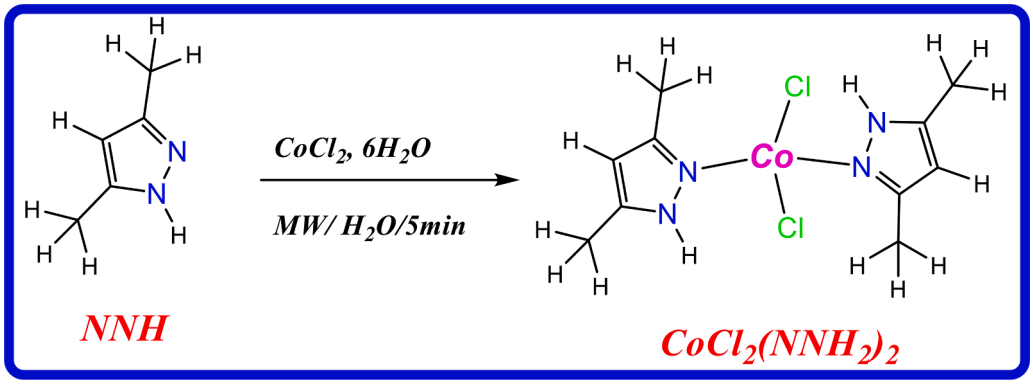

Scheme 1. synthesis of $CoCl_2(NNH)_2$ complex using microwave irradiation.

may be a more effective and potentially safer alternative to existing antimicrobial agents.

Overall, this study provides promising evidence for the potential use of the $CoCl_2(NNH)_2$ complex as an antimicrobial agent, and further research is needed to evaluate its efficacy and safety in clinical settings.

3.8. POM calculation

The young POM (Petra/Osiris/Molinspiration) theory, created and developed by Ben Hadda in cooperation with the American TAACF and NCI centers, was properly designed to predict the most imperative bio-informatics parameters and design of new and simple molecules with specific features pharmacology [7,8,19,20].

The prepared complex $CoCl_2(NNH)_2$ was evaluated to define its pharmacophore sites in agreement with POM rules (Table 4). The characterization of the class, size, and location of pharmacophore sites of the synthesized complex was assessed (Fig. 4). Data of molecular properties, bioactivity scores calculation and toxicities are tabulated in (Table 4 and 5). All results of the calculation are characterized by a good water solubility due to the cLogP=3 lower than 5 (Table 5). The presence of polar zones for NH, $N = N$, Cl, and inorganic part and size of the molecule have affected positively on bioavailability, bioactivity scores and toxicities (Table 4).

The tested complex presents well an antifungal activity and moderate antibacterial activity in comparison with standards (Table 4). These results can be explained by the identification of the pharmacophore sites of the tested complex. Fig. 4 is showing that the tested complex contains many antifungal sites with different sizes ($\mathbf{d_4}$ and $\mathbf{d_5}$) and just two bacterial sites ($\mathbf{d_4}$). Finally, these identifications are in excellent agreement with the experimental part. Therefore, the identification of pharmacophore sites is one of the best ways to select any prepared compounds to its suitable biological applications.

4. Conclusion

Under MW conditions, the deformed tetrahedral $CoCl_2(NNH)_2$ complex was made accessible in under 5 min with no -products high yield reaction. The formation of the desired Td structure was supported by the XRD, FT-IR, CHN-EA (Elemental analysis), UV-visible, and FT-IR results. The theoretical TD-DFT and DFT-IR results agreed with the results of their related experiments, confirming the formation of the [1Co:2NHH] ratio $CoCl_2(NNH)_2$ formula complex. Additionally, XRD and HSA interaction analyses provided strong evidence for the experimental 3D-Td-structure of the intended $CoCl_2(NNH)_2$ complex and the heteromeric R_2^2 *(10) [N—H···Cl]* synthon. Significant activity against *bacteria and fungus* was also shown by the $CoCl_2(NNH)_2$ compound, which was likewise described by the POM theory Scheme 1.

Authorship statement

All individuals who meet the requirements for authorship are listed as authors, and all authors certify that they have contributed sufficiently to the work to assume public responsibility for its content, including involvement in its conception, design, analysis, writing, or revision. As a result, we hereby declare that none of the authors have any conflicts of interest.

Declaration of Competing Interest

The authors declare that they have no conflicts of interest.

Data availability

Data will be made available on request.

Acknowledgments

The author would like to thank Kuwait University and the RSP unit general facilities.

References

[1] A. Titi, I. Warad, S.M. Almutairi, M. Fettouhi, M. Messali, A. Aljuhani, R. Touzani, A. Zarrouk, One-pot liquid microwave-assisted green synthesis of neutral *trans*-$Cl_2Cu(NNOH)_2$: xRD/HSA-interactions, antifungal evaluations, Inorg. Chem. Comm. 122 (2020), 108292.

[2] A. Titi, S.M. Almutairi, R. Touzani, M. Messali, M. Tillard, M.El.K B.Hammouti, D. Eddike, A. Zarrouk, I. Warad, A new mixed pyrazole-diamine/Ni(II) complex, Crystal structure, physicochemical, thermal and antibacterial investigation, J. Mol. Struct. 1236 (2021), 130304.

[3] A. Titi, T. Shiga, H. Oshio, R. Touzani, B. Hammouti, M. Mouslim, I. Warad, Synthesis of novel $Cl_2Co_4L_6$ clusterusing 1-hydroxymethyl-3, 5-dimethylpyrazole (LH) ligand: crystal structure, spectral, thermal, Hirschfeld surface analysis and catalytic oxidation evaluation, J. Mol. Struct. 1199 (2020), 126995.

[4] A. Titi, M. Messali, M.Fettouhi R.Touzani, A. Zarrouk, N. Al-Zaqri, A. Alsalme, F. A. Alharthi, A. Alsyahi, I. Warad, Synthesis of novel tetra (μ3-Methoxo) bridged with [Cu(II)-O-Cd(II)] double-open-cubane cluster: xRD/HSA-Interactions, spectral and oxidizing properties, Inter. J. Mol. Sci 21 (22) (2020) 8787.

[5] A. Titi, H. Oshio, R. Touzani, M. Mouslim, A. Zarrouk, B. Hammouti, N. Al-Zaqri, A. Alsalme, I. Warad, Synthesis and XRD of novel Ni 4 (μ 3-O) 4 Twist cubane cluster using three NNO mixed ligands: hirshfeld, spectral, thermal and oxidation properties, J. Clus. Sci 32 (2021) 227.

[6] A. Titi, R. Touzani, A. Moliterni, C. Giacobbe, F. Baldassarre, M. Taleb, N. Al-Zaqri, A. Zarrouk, I. Warad, Ultrasonic clusterization process to prepare $[(NNCO)_6Co_4Cl_2]$ as a novel double-open-Co_4O_6 Cubane Cluster: SXRD Interactions, DFT, physicochemical, thermal behaviors, and biomimicking of catecholase activity, ACS Omega 7 (2022) 32949.

[7] A. Titi, M. Messali, B.A. Alqurashy, R. Touzani, T. Shiga, H. Oshio, M. Fettouhi, M. Rajabi, F.A. Almalki, T.B. Hadda, Synthesis, characterization, X-Ray crystal study and bioctivities of pyrazole derivatives: identification of antitumor, antifungal and antibacterial pharmacophore sites, J. Mol. Struct. 1205 (2020), 127625.

[8] A. Titi, R. Touzani, A. Moliterni, T.B. Hadda, M. Messali, R. Benabbes, M. Berredjem, Synthesis, structural, biocomputational modeling and antifungal activity of novel armed pyrazoles, J. Mol. Struct. 1264 (2022), 133156.

[9] H. Xu, L. Xingxing, S. Tengda, Q. He, Q. Yue, L. Yufan, Y. Xinling, Z. Li, L. Yun, 1, 2, 3, 4-tetrahydroisoquinoline-based schiff bases as laccase inhibitors: synthesis and biological activity, 3D-QSAR, and molecular docking studies, Z. Xiaoming. Novel 1285 (2023), 135526.

[10] T. Dontsova, A. Tetiana, V.N. Svitlana. I. M. Astrelin, Metaloxide nanomaterials and nanocomposites of ecological purpose, J. Nanomaterials 2019 (2019) 1.

[11] K.M. Leahy, O.L. Richard, W. Yu, B.S. Zweifel, T.K. Alane, L.M. Jaime, Cyclooxygenase-2 inhibition by celecoxib reduces proliferation and induces apoptosis in angiogenic endothelial cells *in vivo*, Cancer Res. 62 (2002) 625.

[12] H. Chen, L. Zhengming, H. Yufeng, Synthesis and Fungicidal Activity against Rhizoctonia s olani of 2-Alkyl (Alkylthio)-5-pyrazolyl-1, 3, 4-oxadiazoles (Thiadiazoles), J. Agric. Food. Chem. 48 (2000) 5312.

[13] M.El. Boutaybi, A. Titi, A.YA. Alzahrani, Z. Bahari, M. Tillard, B. Hammouti, R. Touzani, Aerial Oxidation of Phenol/Catechol in the Presence of Catalytic Amounts of $[(Cl)_2Mn(RCOOET)]$, RCOOET=Ethyl-5-Methyl-1-(((6-methyl-3-nitropyridin-2-yl)amino)methyl)-1H-pyrazole-3-carboxylate, Catalysts 12 (2022) 1642.

[14] A. Titi, K. Zaidi, A.Y.A Alzahrani, M. El Kodadi, El.B. Yousfi, A. Moliterni, B. Hammouti, R. Touzani, M. Abboud, New *in situ* catalysts based on nitro functional pyrazole derivatives and copper (II) salts for promoting oxidation of catechol to o-quinone, Catalysts 13 (2023) 162.

[15] S. Jodeh, J. Ahlam, H. Ghadir, M. Younes, S.S. Zaki, R. Smaail, M. Valbonë, B. Avni, T. Said, D. Omar, Experimental and theoretical study for removal of trimethoprim from wastewater using organically modified silica with pyrazole-3-carbaldehyde bridged to copper ions, BMC Chem 16 (2022) 17.

[16] R. Saddik, I.H. Rafik, T. Said, R. Othmane, R. Smaail, I.Z. Maha, B.B. Abir, H. M. Vijay, M.A. Zainab, Mesoporous Silica Modified with 2-Phenylimidazo [1, 2-a] pyridine-3-carbaldehyde as an Effective Adsorbent for Cu(II) from Aqueous Solutions: a Combined Experimental and Theoretical Study, Molecules 27 (2022) 5168.

[17] G. Laadam, M. El Faydy, F. Benhiba, A. Titi, H. Amegroud, Arej S. Al-Gorair, H. Hawsawi, Outstanding anti-corrosion performance of two pyrazole derivatives on carbon steel in acidic medium: experimental and quantum-chemical examinations, J. Mole. Liq. (2023), 121268.

[18] G. Laadam, F. Benhiba, M. El Faydy, A. Titi, Arej S. Al-Gorair, Mubark Alshareef, H. Hawsawi, Anti-corrosion performance of novel pyrazole derivative for carbon steel corrosion in 1M HCl: computational and experimental studies, Inorg. Chem. Comm. 145 (2022), 109963.

[19] A. Titi, S.M. Almutairi, A.F. Alrefaei, S. Manoharadas, B.A. Alqurashy, P.K. Sahu, B. Hammouti, R. Touzani, M. Messali, I. Ali, Novel phenethylimidazolium based ionic liquids: design, microwave synthesis, in-silico, modeling and biological evaluation studies, J. Mol. Liq. 315 (2020), 113778.

[20] T.B. Hadda, V. Rastija, F. AlMalki, A. Titi, R. Touzani, Y.N. Mabkhot, K. Shah, A. Zarrouk, B S, Petra/Osiris/Molinspiration and molecular docking analyses of 3-hydroxy-indolin-2-one derivatives as potential antiviral agents, Curr. Comp. Aid. Drug Desi. 17 (2021) 123.

[21] Bruker Apex3 v2017.3-0, SAINT V8.38A, Bruker AXS Inc.: Madison (WI), USA, 2013/2014 (2017).

[22] L. Krause, R. Herbst-Irmer, G.M. Sheldrick, D. Stalke, Comparison of silver and molybdenum microfocus X-ray sources for single-crystal structure determination, J. Appl. Crystallogr. 48 (2015) 3.

[23] G.M. Sheldrick, SHELXT–Integrated space-group and crystal-structure determination, Acta Crystall. Sect. A Found. Adv. 71 (2015) 3.

[24] L.J. Farrugia, ORTEP-3 for windows-a version of ortep-III with a graphical user interface (GUI), J. Appl.Crystall. 30 (1997) 565.

[25] S.Y. Haoyu, X. He, S.L. Li, D.G. Truhlar, MN15: a Kohn–Sham global-hybrid exchange–correlation density functional with broad accuracy for multi-reference and single-reference systems and noncovalent interactions, Chem. Sci. 7 (2016) 5032.

[26] I. Badran, T. Said, R. Smaail, Z. Abdelkader, I. Warad, Experimental and first-principles study of a new hydrazine derivative for DSSC applications, J. Mol. Struct. 1229 (2021), 129799.

[27] N. Mardirossian, M. Head-Gordon, Thirty years of density functional theory in computational chemistry: an overview and extensive assessment of 200 density functionals, Mol. Phys. 115 (2017) 2315.

[28] R. Peverati, D.G. Truhlar, Quest for a universal density functional: the accuracy of density functionals across a broad spectrum of databases in chemistry and physics, Philos. Trans. Royal Soc A Math. Phys. Eng. Sci. 372 (2011), 20120476.

[29] L. Goerigk, H. Andreas, B. Christoph, E. Stephan, N. Asim, G. Stefan, A look at the density functional theory zoo with the advanced GMTKN55 database for general main group thermochemistry, kinetics and noncovalent interactions, Phys. Chem. Chem. Phys. 19 (2017) 32184.

[30] I. Badran, A. Rauk, Y. Shi, New orbital symmetry-allowed route for cycloreversion of silacyclobutane and its methyl derivatives, J. Phys. Chem. A 123 (9) (2019) 1749.

[31] I. Badran, A. Rauk, Y.J. Shi, Theoretical Study on the ring-opening of 1,3-disila-cyclobutane and H2 elimination, J. Phys. Chem. A 116 (2012) 11806.

[32] I. Badran, S. Yujun, A kinetic study of the gas-phase reactions of 1-methylsilacyclobutane in hot wire chemical vapor deposition, Phys. Chem. Chem. Phys. 20 (2018) 75.

[33] M.J. Frisch, G.W. Trucks, H.B. Schlegel, G.E. Scuseria, M.A. Robb, J.R. Cheeseman, G. Scalmani, V. Barone, G.A. Petersson, H. Nakatsuji, X. Li, M. Caricato, A.V. Marenich, J. Bloino, B.G. Janesko, R. Gomperts, B. Mennucci, H.P. Hratchian, J.V. Ortiz, A.F. Izmaylov, J.L. Sonnenberg Williams, F. Ding, F. Lipparini, F. Egidi, J. Goings, B. Peng, A. Petrone, T. Henderson, D. Ranasinghe, V.G. Zakrzewski, J. Gao, N. Rega, G. Zheng, W. Liang, M. Hada, M. Ehara, K. Toyota, R. Fukuda, J. Hasegawa, M. Ishida, T. Nakajima, Y. Honda, O. Kitao, H. Nakai, T. Vreven, K. Throssell, J.A. Montgomery Jr., J.E. Peralta, F. Ogliaro, M.J. Bearpark, J.J. Heyd, E.N. Brothers, K.N. Kudin, V.N. Staroverov, T.A. Keith, R. Kobayashi, J. Normand, K. Raghavachari, A.P. Rendell, J.C. Burant, S.S. Iyengar, J. Tomasi, M. Cossi, J.M. Millam, M. Klene, C. Adamo, R. Cammi, J.W. Ochterski, R.L. Martin, K. Morokuma, O. Farkas, J.B. Foresman, D.J. Fox, Gaussian 16 Rev. C.01, Wallingford, CT, (2016).

[34] R. Dennington, A.K. Todd, M.M. John, GaussView Version 6, Semichem Inc, Shawnee Mission KS (2019).

[35] X. Li, X. Xu, X. You, D.G. Truhlar, Benchmark calculations for bond dissociation enthalpies of unsaturated methyl esters and the bond dissociation enthalpies of methyl linolenate, J. Phys. Chem. A 120 (2016) 4025.

[36] J.D. Silversides, C.A. Cheryll, J.A. Stephen, Copper(II) cyclam-based complexes for radiopharmaceutical applications: synthesis and structural analysis, Dalton transactions 9 (2007) 971–978.

[37] S. Shin, N. Saira, L. Hyosun, Polymerizations of methyl methacrylate and rac-lactide by 4-coordinate cobalt(II) complexes supported by N′-substituted N,N′,N-bis ((1H-pyrazol-1-yl)methyl)amine derivatives, Polyhedron 141 (2018) 309.

[38] I. Badran, L. Abdallah, R. Mubarakeh, I. Warad, Effect of alkyl derivation on the chemical and antibacterial properties of newly synthesized Cu(II)-diamine complexes, Moro. J. Chem. 7 (2019) 7.